CHAPTER-7

GEOCHRONOLOGY

"*Geologist have a saying – Rocks remember*."
Neil Armstrong

PART – A: Monazite Geochronology

7.A.1 Introduction

This chapter employs U-Th-Pb monazite (high-grade gneiss) and U-Pb zircon (mafic and pelitic granulites) dating methods to acquire absolute ages poly-metamorphic events of metamorphic rocks. Monazite is a minor mineral and has been discovered by [357], a curiosity that is one of the rare minerals commonly found in pegmatites. The most extensive monazite study was done by [358], which mainly consisted of thorium and rare earth elements. The large size of monazite crystals is preserved in various museums, mainly Madagascar, USA, Sri Lanka and Arendal (Norway). Monazite was first identified as radioactive minerals by Marie and Pierre Curie [359].

Since Th-U-Pb_T chemical dating was first applied in thorite and uraninite [360]. Monazite dating with electron microprobe analyzer (EPMA) has been extensively used for metamorphic and igneous rocks from the last few decades [134, 361-364]. Monazite mineral is a phosphate of LREE [(Ce, La, Nd, Th) PO_4], with abundant U, Th and little Pb [133]. The rapid accumulation of radiogenic lead (*Pb) is possible to a required level, analyzed with an electron probe [134]. Pb diffusion is very low in the monazite under the crustal environment, whereas it presents relatively broad and homogeneously distribution [143, 365, 366]. Monazite dating with the help of an electron microprobe has been performed by several researchers based on the abundance of Th, U and Pb [134, 151, 361, 362, 367]. Monazite presents in several igneous, metamorphic, and diverse

hydrothermal rocks as accessory minerals, and also presents in psammitic sediments and sedimentary rocks as a detritic phase [368]. An uncommon existence of monazite is recognized in lunar basalts by [369]. The EPMA monazite dating technique is a reliable technique to identify the recorded history of polymetamorphic events [16, 70, 370, 371]. Monazite dating and mineral chemistry are powerful features for dealing with geological problems, including the superposition of lithosphere and petrological evolution during geological history.

The analysis of chemical ages and statistical calculation in monazite was discussed by [134], while [151] derived an age distribution map for the first time of particular monazite crystal. EPMA dating technique is based on quantification of Th, U, Pb with appropriate accuracy and precision. Various factors like; sample preparation, instrument setup, and calibration with current intensity play a crucial role unless data treatment introduces several error types [372-374].

7.A.2 Theoretical foundation and premises

Monazite chemical dating was first performed by [361, 362], based on the CHIME (CHemical Isochron MEthod). It can be used with both Th-rich phases and more U rich phases, such as zircon or xenotime. The theoretical method is similar to the chemical ageing of U-Th minerals used in earlier efforts in geochronology. This allows determining a monazite crystal's geochronology from a point location or a set of analyses. When multiple analyzes determine a single age, the method will be corrected for non-radiogenic lead. The relationship between the wt% of UO_2, ThO_2 and PbO in a Th- or U-rich mineral, and the age of that mineral, can be defined by equation (1) [361, 375]. This is solved with a preliminary estimation for age, and then calculates an amount

corresponding to PbO. A new and improved age is then estimated, and the PbO* value is recomputed. This repeating process continues until the PbO value converges at the measured value. In the first step, an apparent age (t) is obtained from the set of UO_2, ThO_2 and PbO (wt %) values by solving the equation:

$$\frac{PbO}{W_{Pb}} = \frac{\mathrm{ThO_2}}{\mathrm{W}_{Th}} \{exp(\lambda_2\, t) - 1\} + \frac{\mathrm{UO_2}}{W_U} \left\{\frac{exp(\lambda_5 t) + 138\, exp(\lambda_8 t)}{139} - 1\right\} \quad (1)$$

Where: W = molecular wt. of oxides; W_U = 270, W_{Th} = 264, W_{Pb} = 224 (for monazite) & 222 (for zircon and xenotime). λ is the decay constant; (232) λ_2 = 4.9475 × 10-11/Year, (235) λ_5 = 9.8485 × 10-10/Year, (238) λ_8 = 1.55125 × 10-10/Year [376]. 't' is the apparent age determined from each analysis.

$$ThO_2^* = ThO_2 + \frac{UO_2\, W_{Th}}{W_U\{exp(\lambda_2 t) - 1\}} \left\{\frac{\exp(\lambda_5 t) + 138\exp(\lambda_8 t)}{139} - 1\right\} \quad (2)$$

$$UO_2^* = UO_2 + \frac{139\, ThO_2\, W_U\{ex\, p(\lambda_2 t) - 1\}}{W_{Th}\{exp(\lambda_5 t) + 138\, exp(\lambda_8 t) - 139\}} \quad (2')$$

ThO_2* is the equivalent amount of ThO_2 that would be required to produce the measured amount of PbO, if there was no UO_2 in the mineral. UO_2* is the equivalent amount of UO_2 that would be required to produce the measured amount of PbO, if there was no ThO_2 in the mineral.

$$PbO = m\, ThO_2^* + b \quad (monazite) \quad (3)$$

$$PbO = m\, UO_2^* + b \quad (Zircon\ and\ Xenotime) \quad (3')$$

If individual parts of a single mineral crystal are monogenetic, it contains the similar quantity of initial Pb, but the dissimilar quantity of Th and U, and persists in a closed system, where "m" is the slope of the least square fit curve for analytical data and "b" is the intercept of the least square fit curve.

T_S is the age determined from the slope of PbO versus ThO_2* (or UO_2*). The best-fit regression line is defined with the method recommended by [377], taking into account uncertainties in probe analyses, and determine the first approximation of age (T) from the slope (m) of equations:

$$T_s = \frac{1}{\lambda_2} In\ (1 + m)\ \frac{W_{Th}}{W_{Pb}} \quad (4)$$

$$m\ \frac{W_{Th}}{W_{Pb}} = \frac{\exp(\lambda_5 T_s) + 138\ \exp(\lambda_8\ T_s)}{139} - 1 \quad (5)$$

The apparent age (t) can be replaced with the second approximation age, and the second approximation (T) age in a similar way. The line's intercept (b) is expected to mark the initial PbO value.

In-situ dating of monazite grain with electron microprobe has several advantages which are given below: (1) Since it is non-destructive the same thin section which was used for dating of the metamorphic events can be used for the textural relationship of the minerals in relation with time and deformation [363, 378], (2) It has a high spatial resolution (1-3µm) which enable us to analyze compositional inhomogeneities and zonation even on small grain size, and (3) can obtain results in a short period without separation of an isotope.

7.A.3 Analytical techniques

The analytical work was performed using an electron probe microanalysis (EPMA) on a CAMECA SX five instrument at the DST-SERB National Facility, Department of Geology (CAS), Institute of Science, BHU. The thin polished section was coated with a 20 nm thin layer of carbon using a LEICA-EM ACE200 carbon coater instrument. The EPMA instrument CAMECA SX Five was operated with SX Five

software at an accelerated voltage of 15 kV and a current of 200 nA with a LaB6 source in the electron gun for electron beam generation, which is based on a new analytical protocol for the U–Th–Pb chemical dating of monazite [379]. Andradite is used as a natural silicate mineral to verify crystal positions using an internal standard (SP2-LiF, SP3-LPET, SP4-LTAP and SP5-PET) with suitable wavelength dispersive spectrometers (SP #) using the CAMECA SX-Five instrument. The following X-ray lines were used in the analyses: F–Ka, Na–Ka, Mg–Ka, Al–Ka, Si–Ka, P–Ka, Cl–Ka, K–Ka, Ca–Ka, Ti–Ka, Cr–Ka, Mn–Ka, Fe–Ka, Ni–Ka and Ba–La. Natural mineral standards: fluorite, halite, periclase, corundum, wollastonite, apatite, orthoclase, rutile, chromite, rhodonite, hematite and barite; Ni pure metal standard was supplied by CAMECA-AMETEK which was used for routine calibration and quantification. Quantification of rare-earth element (REE) analysis in monazite mineral phases and U, Th and Y elemental X-ray mapping of monazite grains was obtained at an accelerating 20 kV voltage currents of a beam are 200 nA, at 0.5 lm/pixel spatial resolution. The following X-ray lines were used in the analyses: Y–La, La–La, Ce–La, Pr–La, Nd–La, Sm–La, Eu–La, Th–Ma and U–Ma. All REE analysis was carried out on aLiF crystal attached with SP2 and Pb, Th and U were analyzed with an LPET crystal connected with the SP3 spectrometer in a CAMECA-SX five EPMA instrument. Synthetic glass standards of all REE (La to U) supplied by CAMECA AMETEK were used for routine calibration and quantification.

Scanning electron microscope (SEM) analysis was performed at the DST-SERB National Facility, Department of Geology (CAS), Institute of Science, BHU. The SEM instrument was operated at an accelerated voltage of 15 kV and a current of 200 nA.

7.A.4 Sample preparation and identification of monazite

Preparation of polished thin-sections has been done for petrographic investigation. The purpose of petrography is to find out the position of monazite crystals in the host mineral or matrix, which helps interpret age. Optical microscopes have a low resolution for identifying monazite, so SEM plays an essential role in detecting monazite. Monazite occurs as an accessory phase in the rocks. Zircon causes some confusion with monazite to identify monazite grains under a petrological microscope. Monazite and zircon have some important diagnostic features and can be distinguished by their characteristics [134]: (1) The zircon crystals have distinct two pyramid prismatic, but monazite crystals display only single pyramid if present; (2) monazite crystals have a thin laminar cleavage (100) while zircons have coarse (if any), similar to pyroxenes; (3) the extinction angle of zircon is very distinctive 0º, but monazite has 5–10º; (4) if a crystal exhibits zoning in plane-polarized light, it may be a zircon; (5) zircon's refractive index (n = 1.92–2.01) is higher than monazite (n = 1.77–1.85); (6) usually, monazite crystals form rounded, subrounded and anhedral shape, whereas zircon forms prisms as well as euhedral shape. The pleochroic haloes formed by zircons were small, but monazite produced comparatively larger pleochroic haloes in flakes of biotite and cordierite, due to an abundance of Th, i.e., 3.14–7.20 wt%. However, solely on optical properties, monazite and zircon grains cannot be easily distinguished.

The SEM and energy dispersive system (EDS) are authentic instruments for immediate identification of monazite grains. Deprived of EDS, monazite can be recognized in BSE images because it is exceptionally bright (higher atomic number), even higher than that of zircon, leaving only thorite and uraninite [134]. The back-

scattered electron (BSE) images were used to identify the monazite grains from the matrix and garnet. Some separated monazites are also used for mounting on the epoxy resin. The electron microprobe quickly detects the separated mineral through a Th intensity signal. This method's disadvantage is the inability to find the petrographic position of dated crystals, and small crystals (<20–50 μm) are omitted during this separation process.

7.A.5 Textural interpretations of monazite

The analyzed monazite grains are incorporated within porphyroblastic garnet, cordierite, biotite, and matrix (Fig.7.1). Garnet shows compositional variation from the core to the rim with relatively lower Alm and Sps in the core ($Py_{29.5}Alm_{69.5}Grs_{0.7}Sps_{0.3}$) and slightly higher pyrope content than the rim ($Py_{23.3}Alm_{75.4}Grs_{0.6}Sps_{0.7}$) (Fig.5.2). Monazite grains at the core of the garnet (Fig.7.1a) produced older ages in R-91–97, and many monazite grains embedded in the periphery zone (Fig.7.1b) produced younger ages in R-91–96. Garnet is rimmed by cordierite and exhibits a corona texture (Fig.7.1a) consisting of biotite and quartz as inclusion that leads to cordierite formation. Monazite grains are also present in the cordierite, biotite (Fig.7.1c&d), gedrite and matrix which provide younger age. Monazite grains occur as accessory minerals in the matrix and are ubiquitous in both high-grade gneisses; large grains of monazite (60–80 micron) are usually found in high-grade metamorphic rocks [134]. The monazite grains contain 3.14–7.20 wt% of thorium oxide (ThO_2), 0.28–1.52 wt% of uranium oxide (UO_2) and 0.26–0.44 wt% of lead oxide (PbO) in the sample R-91-97. The sample R-91-96 contains 3.53–6.18 wt% of ThO_2, 0.26–1.45 wt% of UO_2 and 0.26–0.46 wt% of (PbO). The normalized cations based on the four oxygen basis are presented in Table 7.1.

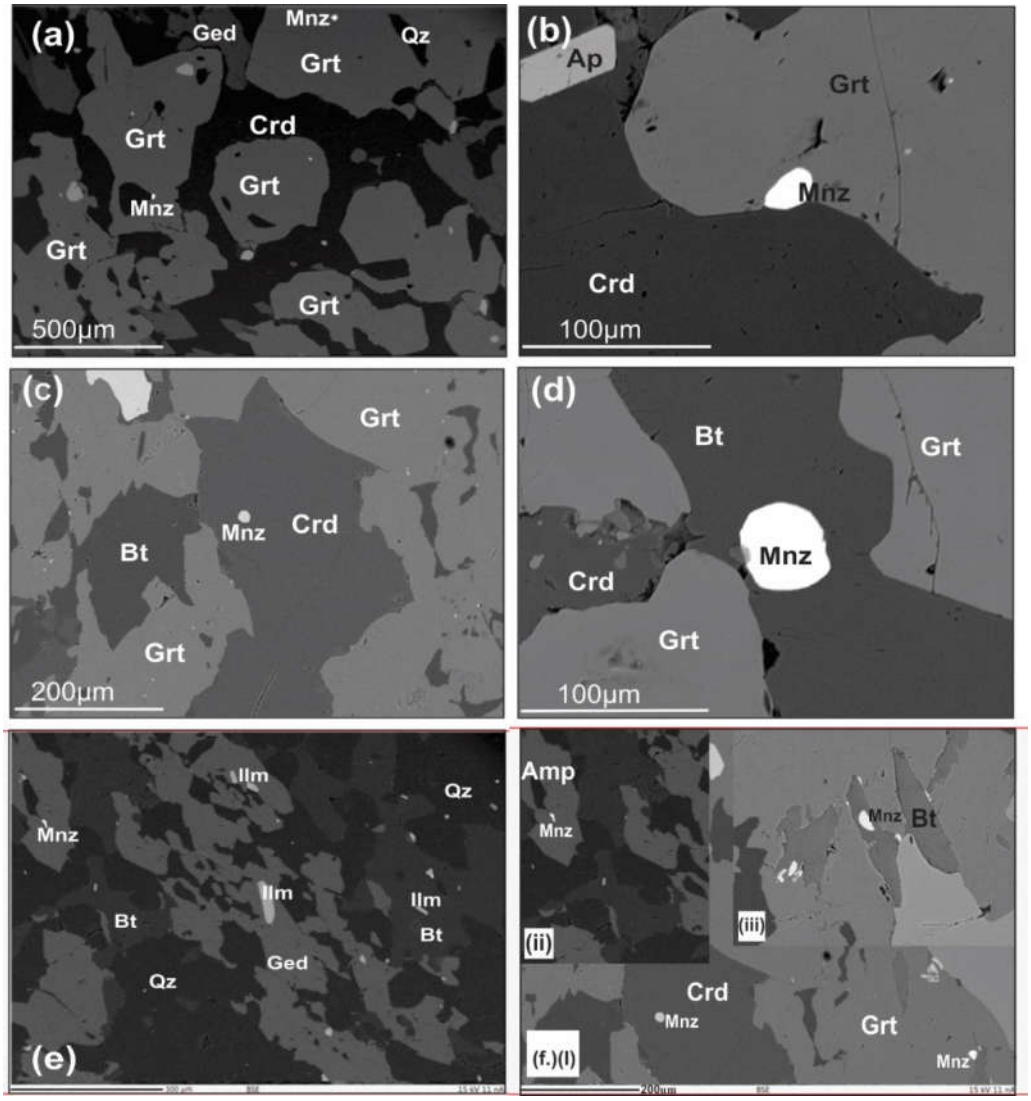

Figure 7.1 Back Scattered Electron (BSE) images are showing the microstructural and textural settings of monazite occurrences in the granulitic gneiss of Daltonganj. (a) Monazite occurring as inclusion within porphyroblastic garnet in R-91-97. (b) Monazite grain occurring as inclusion within the periphery area of garnet in R-91-97. (c) Monazite present as inclusion in the cordierite, Crd is later surrounded by garnet in R-91-96. (d) Monazite occurring as inclusion within biotite in R-91-96. (e) Monazite present in gedrite and garnet. (f) Different images show monazite present in garnet, amphibole, cordierite and biotite.

7.A.6 Sample description and U–Th–Pb systematics

An electron microprobe of thorium (Th)–uranium (U)–lead (Pb) monazite dating principle was applied to obtain the age of granulite rocks from Daltonganj. R-91-97 and R-91-96 samples have been selected for microprobe dating after systematic EPMA-BSE

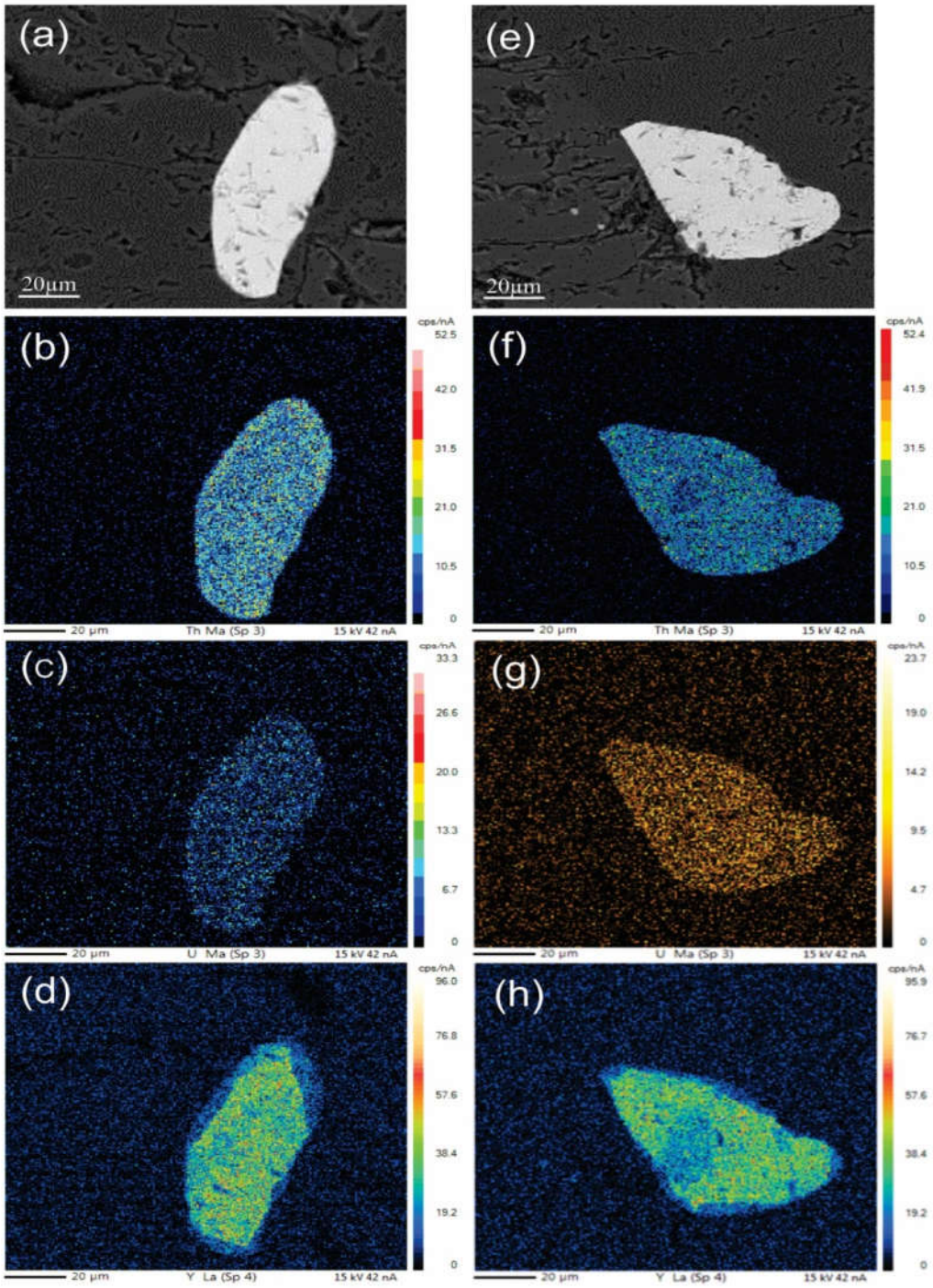

Figure 7.2 Grain-P43 of the R-91-97 sample, (a) BSE image. (b) and (c) X-ray elemental maps documenting the homogeneous pattern of Th and U elements in monazite. (d) X-ray map shows the zoning pattern at the outer part in monazite; wherein grain-P46 of the R-91-96 sample, (e) BSE image, (f) and (g) X-ray elemental maps documenting the homogeneous pattern of Th and U elements in the monazite. (h) X-ray map shows the zoning pattern at the outer part as well as the core of monazite**.**

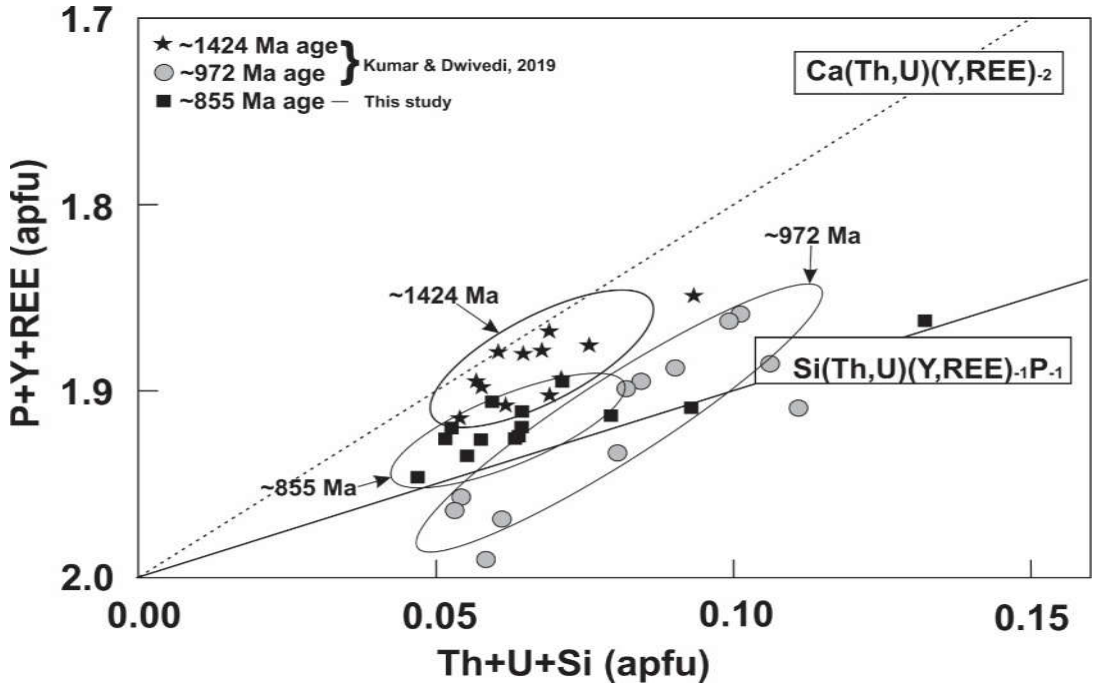

Figure 7.3. The bivariate plot shows the variation in the composition of monazite of three different age domain from Daltonganj (CGGC). ~1424 Ma age enriched in brabantite and ~972 Ma age rich in huttonite, whereas ~855 Ma age lie between both substitution vector.

imaging. Monazite grains are of diameter (70–80 µm) and are compositionally homogeneous (Fig.7.2). Monazite grains show the homogeneous compositional domain demarcated by the BSE images and X-ray elemental mapping. The X-ray elemental maps of some selective monazite grains P43 of R-91-97 and P46 of R-91-96 are shown in Figure 7.2. Both P43 and P46 monazite grains occur as inclusions in the garnet porphyroblast and are relatively poor in yttrium (Y) elemental composition at the outer rim margin compared to the core (Figs.7.2d&h). The partitioning of yttrium (Y) in monazite is directly linked to growth or consumption by peritectic garnet [16, 136]. However, U and Th X-ray elemental maps show homogeneous composition in both the grains (Figs.7.2b, c, f&g). U and Th were found together with Pb in both huttonite and brabantite substitutions. Monazite shows the compositional variation between Th (+Ca

and Si) and Y (+HREE) and reflects the various substitutions: brabantite substitution ($Th^{4+} + Ca^{2+} = 2REE^{3+}$; [380]) and huttonite substitution ($Th^{4+} + Si^{4+} = LREE^{3+} + P^{5+}$; [381]). The variation of brabantite vs huttonite exchange operation is presented in the plot of Th + U + Si vs REE + Y + P (Fig.7.3). All monazite grains contained negligible SiO_2. However, they have sufficient amounts of Ca that determine the amount of brabantite substitution (Th/U+ Ca ↔ 2REE). Here, the brabantite substitution is dominant in monazites. Older (1424 Ma) monazite has an affinity toward brabantite substitution, and huttonite substitution has been shown in monazite aged 972 Ma, while younger age (855 Ma) lies between the intermediates of both substitutions.

7.A.7 Electron microprobe dating

Electron microprobe dating is an efficient investigative tool to find the age of metamorphic events and deformation [151]. Here, EPMA monazite geochronology was conducted to explore the age and establish the history of the development of the granulite of Daltonganj. Monazites vary in shape from anhedral to subhedral or rounded and size from small (10–30 µm) to large grain (60–80 µm). It occurs as inclusion within the garnet and matrix. Estimation of age and uncertainties are compared from different monazite grains, and the events of monazite growth were interpreted as recorded from the Daltonganj. EPMA ages were obtained from various monazite mineral grains from two different granulite samples. The Th–U–Pb values from different monazite grains from R-91-97 and R-91-96 samples are given in table 7.1. EPMA dating has generated three age domains, the weighted average age distribution and probability density plot were obtained using the ISOPLOT program [382] as depicted in figure 7.5a–j. The analysis of sample R-91-97 produced an age population at 1424 ± 64 Ma (Fig.7.5a&b)

and 972 ± 28 Ma, with 95% confidence (Fig.7.5c&d). The sample R-91-96 has an age population of 1390 ± 56Ma (Fig.7.5e&f) and 962 ± 15 Ma, with 95% confidence (Fig.7.5g&h). However, this third age domain represents the youngest monazite age from high-grade gneiss, ranging from 712 ± 60 to 906 ± 58 Ma, with the weighted average age provides an age of 855 ± 31Ma with 95% confidence (Fig.7.5i&j). The electron microprobe dating of monazite grains has generated a three-age domain from both rocks, which lies around the Mesoproterozoic and Neoproterozoic ages.

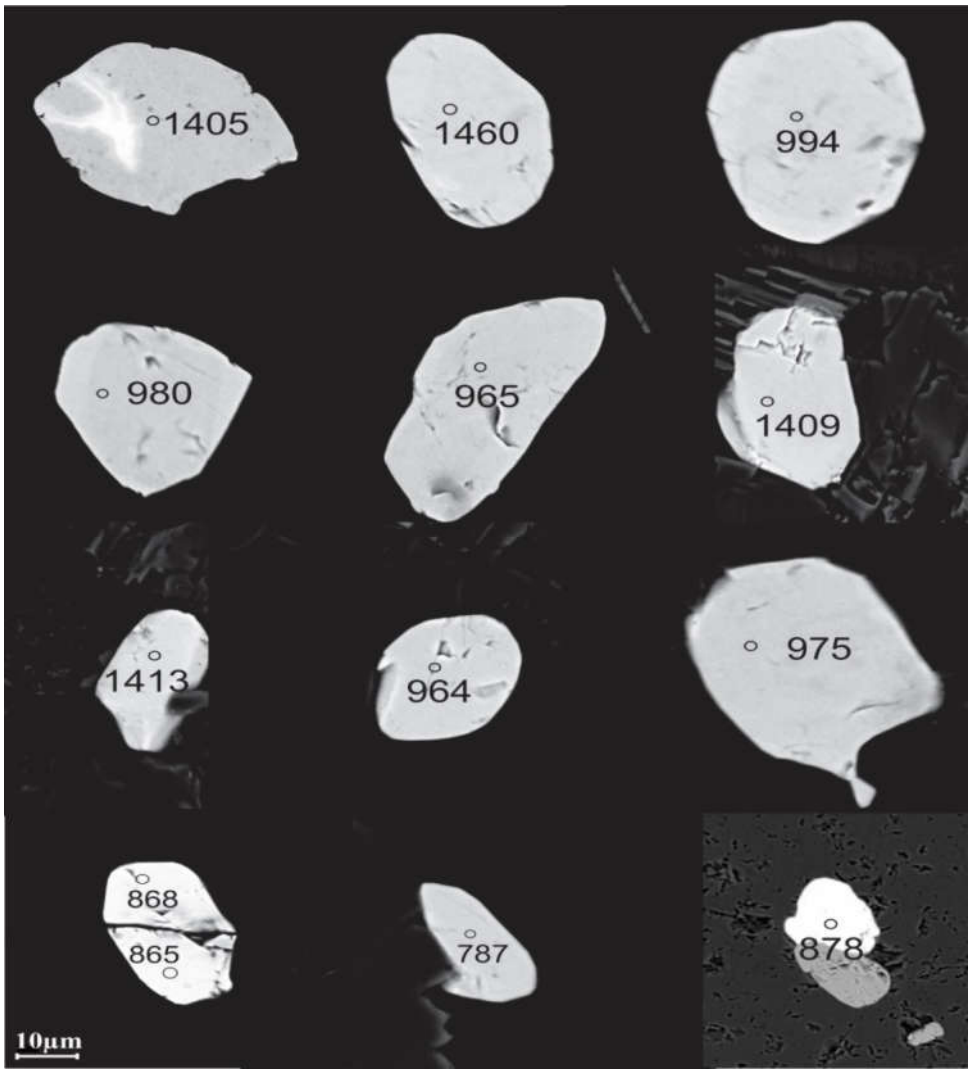

Figure 7.4 Represents the backscattered images (BSE-SEM) of different monazite grains from two rock samples.

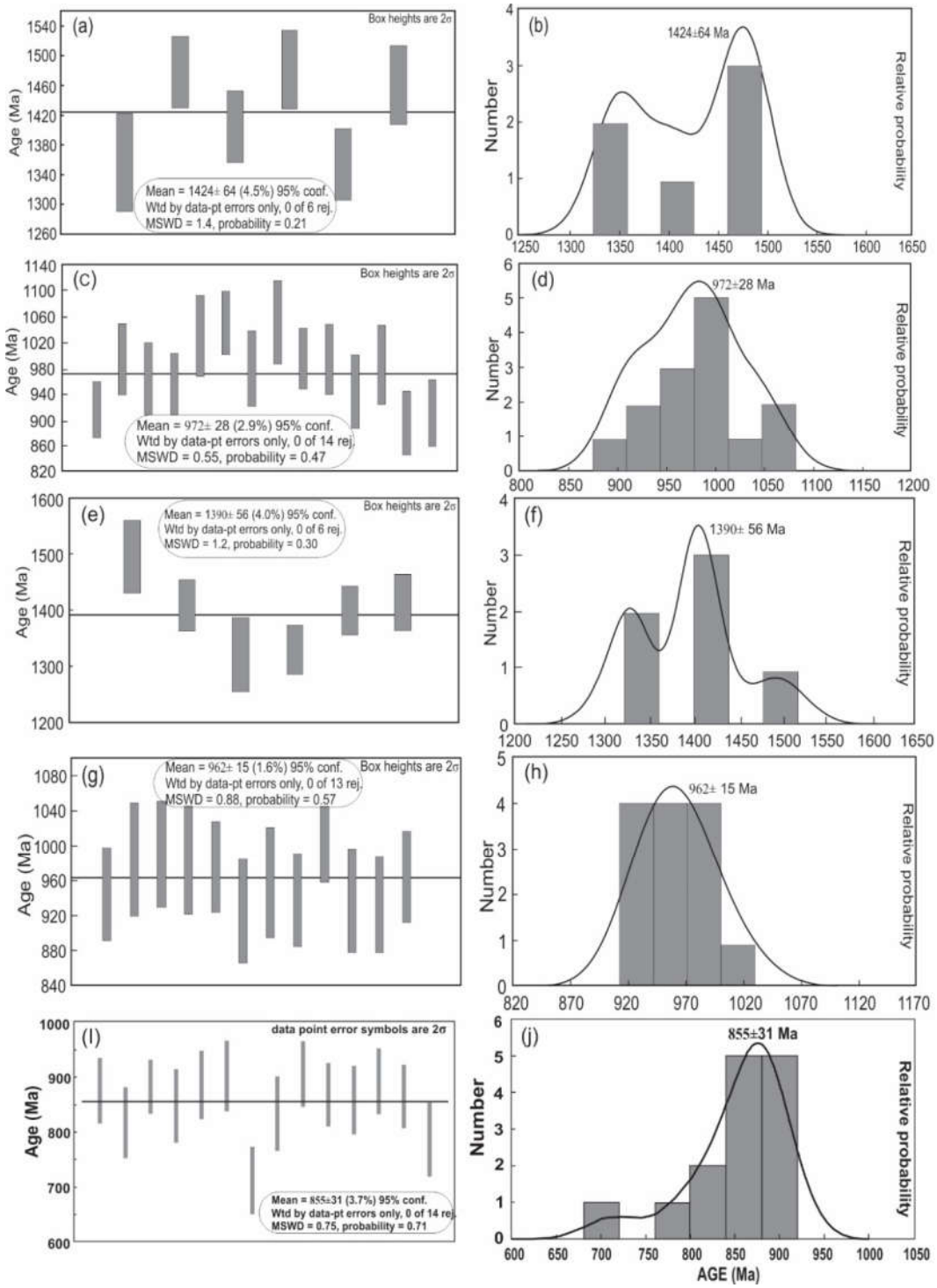

Figure 7.5 (a), (c), (e), (g) and (i) Weighted-average ages; (b), (d), (f), (h) and (j) Probability–density ages of two distinct age domains from the R-91-97 (a,b,c,d) and R-91-96 (e,f,g,h) rock sample, and youngest age for from both samples (I and j) with 2σ uncertainty, different numbers of point analysis and MSWD (mean square of weighted deviates) for monazite from the Daltonganj area of the CGGC, plotted with the ISOPLOT program [382].

PART- B: Zircon Geochronology

7.B.1 Radioactive decay mechanisms

An unstable parent isotope decays through the intermediate isotope (unstable) product to form a stable daughter isotope. The decay rate is free from exterior conditions and is continuous over time. It is depicted as half-life ($t_{1/2}$), which is the interference of time whenever half of the parent radiogenic isotopes are decayed. The radioactive isotope is shown through a series of decay mechanisms:

(1) α- decay: Parent isotope atom emits 2- protons and 2- neutrons (a He nucleus).

i.e. ${}^{A}_{Z}X \rightarrow {}^{A-4}_{Z-2}Y + \alpha + Q$ (6).

(2) β- decay: A parent isotope produces a positron (β^+ decay) or electron (β^- decay), and an electron antineutrino ($\bar{\upsilon}$). Here, a neutron converts to a proton or vice versa, changing the nucleus charge but preserving the same number of nucleons.

${}^{A}_{Z}X \rightarrow {}^{A}_{Z+1}Y + \beta^- + \bar{\nu} + Q\ (\beta^- decay);\ {}^{A}_{Z}X \rightarrow {}^{A}_{Z-1}Y + \beta^+ + \bar{\nu} + Q\ (\beta^+ decay)$ (7)

(3) γ- decay: the nucleus emits a high energy photon as it changes from high energy state to low energy state. In this process, the number of nucleons does not change, so the parent and daughter atoms are the same.

(4) Electron (e^-) capture: It (usually from the K- or L- electron shells) is a consequence in which a proton converted into a neutron and simultaneous emission of an e^- neutrino.

(5) Spontaneous fission: A rare form of decay occurs in the heaviest nuclei (e.g. ^{238}U) in which the nucleus splits into two unequal lighter nuclei, which are often unstable.

7.B.2 U-Pb Systematics

Zircon ($ZrSiO_4$) is the most usable mineral for geochronological studies using U-Pb isotopic systematics [383], while monazite, xenotime, allanite, uraninite, baddeleyite,

rutile, perovskite, and titanite are also normally dated and zircon age suggests that the age of crystallization and emplacement of magmatic protolith along with deformation and metamorphic events [133, 159, 384-399]. U^{4+} is replaced by Zr^{4+} due to the same ionic radius in Zircon (r Zr^{4+} = 0.80 Å; r U^{4+} = 0.97 Å); while Pb^{4+} has a higher ionic radius and low charge then it is omitted from the chemical structure during crystallization [r Pb^{2+} = 1.17–1.28 Å, r Pb^{4+} = 0.79–0.95 Å (r Pb^{4+} is an extremely rare state)] [400]. Zircon is important for dating igneous episodes as it is available as accessory phases in felsic magmatic rocks and mafic intrusives. It acts as a robust mineral that can persist during magmatism, metamorphic events, erosion and sedimentation, and still maintain its crystallization age. The zircon's crystallization age is calculated by the Concordia diagram [401]. While it is the prime objective of its ability to produce robust ages, it also presents some complexities for analyzing data. In general, igneous and metamorphic rocks contain zircons of various generations. The availability of numerous age populations within an investigation leads to a discordant data and requires appropriate analytical approaches and careful interpretation of the results. The upper intercept formed by isotopic analysis of various zircon fractions along the Concordia curve represents the age of crystallization of zircon and the minimum age resulting from crystallization of igneous protoliths, in the same geologic process as zircon and rock crystallization.

The uranium-lead dating is used exclusively to date minerals and rocks formed about 1 to 5000 million years ago. The U-Pb technique is extensively used to determine rocks and minerals [156, 157]. The U-Pb system consists of two isotopic individuals with the same chemical properties but variable decay rates. There are three isotopes in the U:

^{234}U, ^{235}U and ^{238}U; ^{234}U is the intermediary product of the ^{238}U decay chain (Fig.7.6). ^{235}U and ^{238}U decay to produce ^{205}Pb and ^{206}Pb, respectively, represented as the following equations:

$^{238}U \rightarrow {}^{206}Pb + 8\alpha + 6\beta^-$ ($T_{1/2}$ = 4468 million years; [402] (8)

$^{235}U \rightarrow {}^{205}Pb + 7\alpha + 4\beta^-$ ($T_{1/2}$ = 703 million years; [402] (9)

Age is calculated by the geochronometer on the parent-daughter ratio, initial Pb content and decay constant. This dating application is based on the paired decay system and provides an "internal test" on the results of ^{235}U and ^{238}U not being analyzed [400]. This paired decay series develops the Concordia-Discordia plot [401, 403, 404]. A meaningful U-Pb age is attained by following these conditions:

• Uranium was integrated into the atomic structure of minerals during crystallization

• Correct amounts are considered for the initial Pb composition (preferably no initial Pb)

• Minerals have the ability to preserve U, Pb and intermediate daughter isotopes

• An isotopic systems (no loss or no gain of U and Pb)

This is of additional benefit if the mineral is not compatible with incorporating Pb into their structure during crystallization. This offers an excellent U/Pb ratio. However, an open isotopic system of any mineral (rocks) disturbs the dating process. Sometimes, minerals and rocks have generational multi-phases, in which case, U/Pb ratios have variable values that represent mixed ages and require careful interpretation.

7.B.3 Mass Spectrometry

The mass spectrometer is used to calculate the fixed and relative amount of isotopes/ions when passing through a magnetic/electronic field. It has three distinct parts: an ion source, a mass analyzer, and a detector [400]. It works in a closed environment

and operates at high vacuum. U-Pb zircon dating involves three techniques; (1) SIMS: Secondary Ionization Mass Spectrometry, (2) ID-TIMS: Isotope Dilution Thermal Ionization Mass Spectrometry, and (3) LA-ICPMS: Laser Ablation Inductively Coupled Plasma Mass Spectrometry. Here, I have used only the LA-ICPMS analysis.

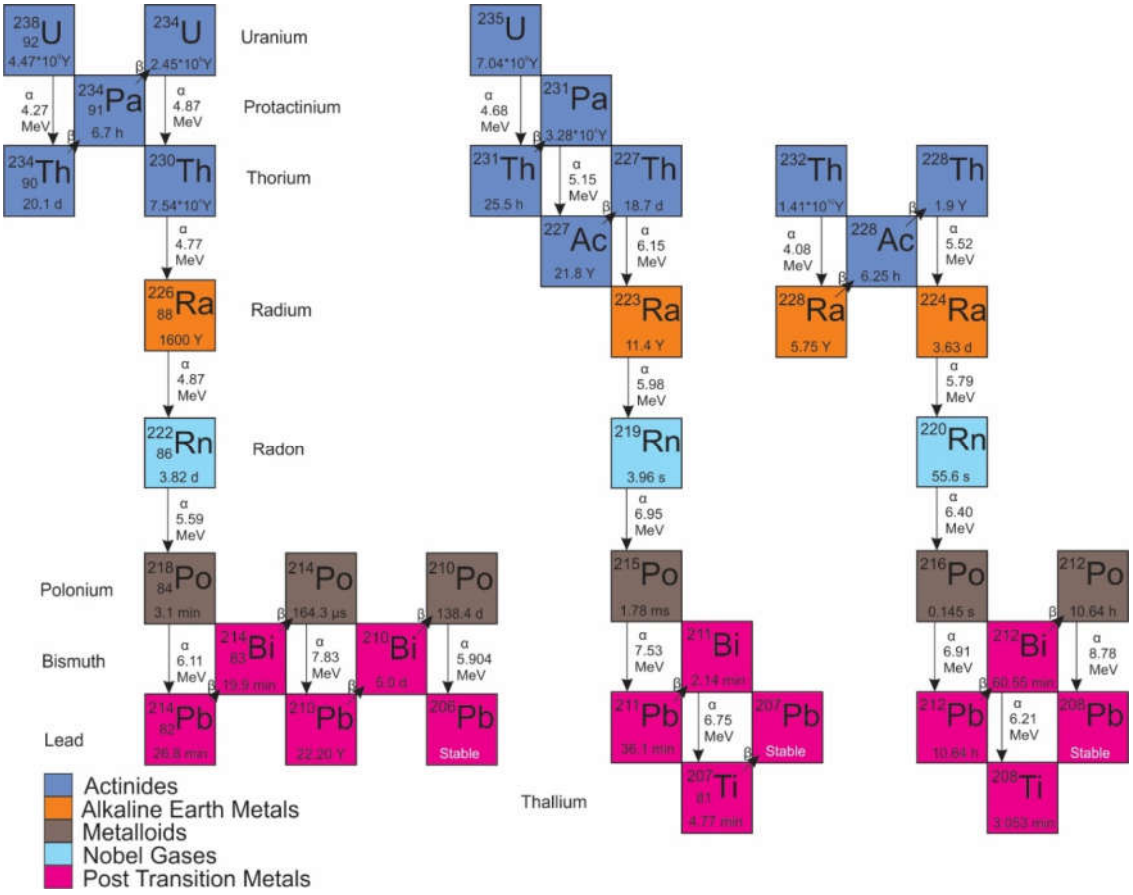

Figure 7.6 Decay chain of ^{238}U to ^{206}Pb, ^{235}U to ^{207}Pb and ^{232}Th to^{208}Pb.

7.B.3.1 LA-ICP-MS

In an LA-ICP-MS, the sample is used in plasma torch with flowing Argon (Ar) gas as two types of modes, namely, an aerosol (from a solution) and as ablation of a solid sample by laser. The sample and Ar gas are ionized Ar gas and sample with energetic electrons. The resulting plasma is transported by flowing Ar gas into the mass

spectrometer. The ions are accelerated into a high-potential electric field and subsequently separated into a magnetic field at a mass-to-charge ratio [405].

LA-ICP-MS instrument is employed on solid samples to elemental and isotopic analysis. LA-ICP-MS is activated with a laser beam focused on the sample surface to produce finer particles; this process known as laser ablation. LA-ICPMS is a fast and inexpensive technique for analyzing U-Pb data and is robust for analyzing the age of magmatism as well as detrital zircon ages [406]. Detrital zircon is used for paleogeographic reconstruction, recognizes tectonically induced drainage systems, identifies magmatic emplacement and further constructs an improved tectonic model of the orogenic belt [407-410]. The major problem is the calibration of the U–Pb ratios, and the problem also arises due to impurities in the Ar gas.

7.B.4 Analytical Technique

Traditional methods separated zircons from various representative samples. Back-scattered images and cathodoluminescence (CL) images were taken using the scanning electron microscope (SEM: JEOL JSM-7500F) at Hiroshima University. These images were helpful in analyzing the size, shape and internal structure of zircon crystals and were used in further evaluation. For LA-ICPMS, U-Pb isotope zircon analysis was executed using 213 nm Nd-YAG Laser (New Wave Research UP-213) coupled with Agilent 7500 ICP-MS at the Department of Earth and Planetary Systems Science, Hiroshima University. A complete analytical procedure was described by [411].

7.B.5. U–Pb zircon geochronology

7.B.5.1 Pelitic granulite

7.B.5.1.a Morphology

The pelitic granulite (D-3) selected for LA-ICPMS U-Pb zircon dating. The cathodoluminescence (CL) imaging of the internal texture of zircons has revealed pelitic granulite consists of both types of zircons i.e., detrital as well as metamorphic. Zircon grains vary from 100–150 µm in size with variable shapes and morphology. Few of the detrital zircons show oscillatory zoning at the core with resorbed boundaries (Figs.7.7a&b). This type of morphology signifies that zircons have a magmatic origin and further experienced by the metamorphic stages [383]. The detrital zircons demarcated by the dark or metamictized xenocrysts core and corrugated boundaries indicate the detrital history of zircon with erosion and sedimentation processes [383]. The detrital zircons show non-luminescent core and mantle and thin but high-luminescent rim portions. Most zircons have high-luminescence at rim and low-luminescence at mantle with a thin layer that is overgrown around the core (Figs.7.7c&d). They are comparatively larger than detrital zircon with an elongated shape and high aspect ratio (4:1), these types of zircon grains had been formed by the successive metamorphic stages [383].

7.B.5.1.b Result

A total of 40 point analysis (Table 7.2) has been done from different zircon grains, showing ≤ 2.5% discordance. The cathodoluminescence (CL) images, Tera-Wasserburg Concordia diagram, and Probability density diagram shown in Figure 7.8. Some of the geochronological data from the oval shape and metamict cores of zircon grains have older age. Most of the older age data lie between 1700–1800 Ma with one data is of 1860.6±31.2 Ma. On relative probability density diagram, it shows 1707.1±8.8 Ma age as the younger detrital age domain (Fig.7.8b). This age group has a high Th/U ratio (>0.2)

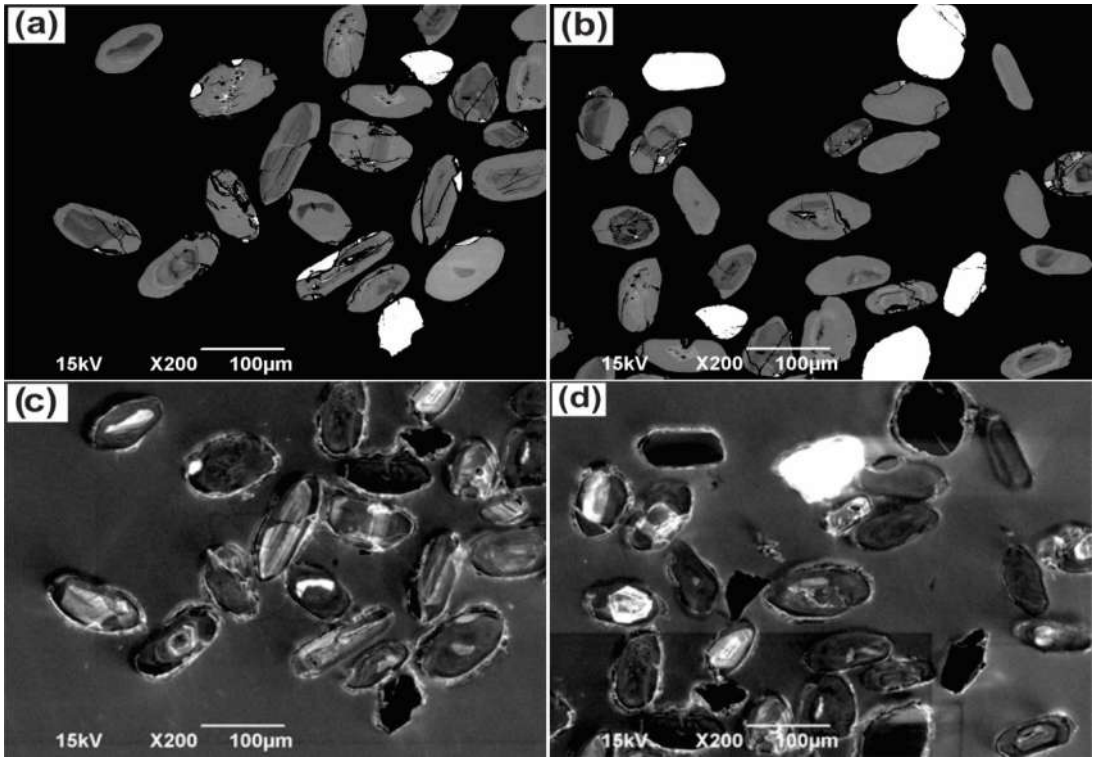

Figure 7.7(a & b) Representative Back-scattered electron (BSE) image; (c & d) Cathodoluminescence (CL) images of zircons with different zoning patterns and metamictised mantle of zircons from pelitic granulites from the Daltonganj area.

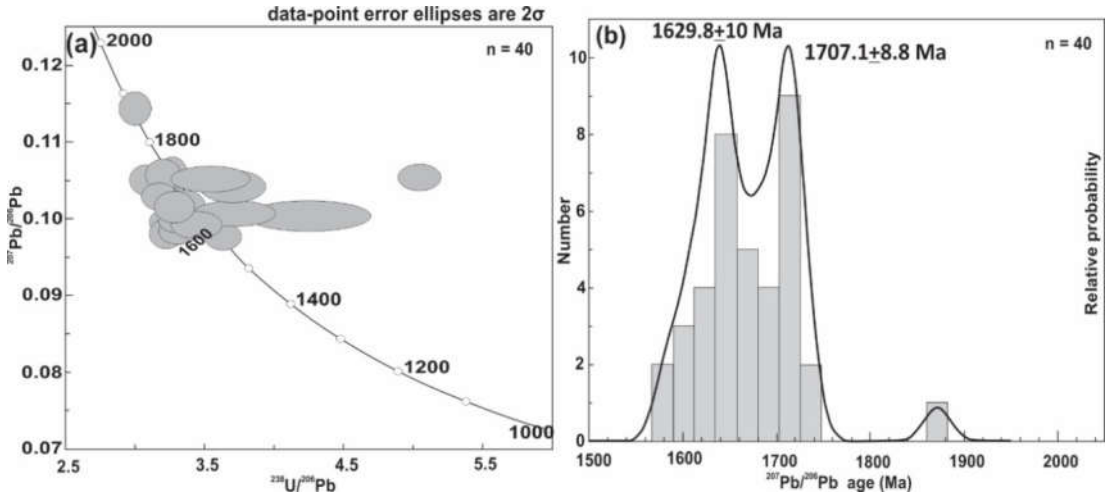

Figure 7.8(a) Analytical data from the pelitic granulite (D-3) plotted in Tera-Wasserburg Concordia graph. (b) Probability density plot of $^{207}Pb/^{206}Pb$ ages showing concordant age: 1707.1±8.8 and 1629.8±10 Ma.

which indicates that detrital zircons formed by the magmatic origin [412]. The sub-rounded and elongated zircon grains recrystallized at different metamorphic events with

having low Th/U ratio (<0.2), these signify that metamorphic origin of zircon [163, 393]. Twenty-six spot analyses of metamorphically formed zircons decipher late Paleoproterozoic age (1629.8±10 Ma).

7.B.5.2 Mafic granulite

7.B.5.2.a Morphology

The zircons are subhedral to ovoid shape, and their colour is light pink to pinkish-white under the binocular microscope. The morphology of crystal varies from elongated and prismatic and ranges from 150–300 μm in size and 1:1–3:1 in length-width ratios (Figs.7.9a&b). Observations with the SEM-CL images reveal that some zircons show oscillatory zoning while other zircons are homogeneous with light luminescence (Figs.7.9c&d). Oscillatory-zoned zircon crystal faces are developed through crystallization process from the melt at high temperature [383]. The analyzed zircon grains are supposed to have generated during the crystallization of the mafic magma.

7.B.5.2.b Result

A total of forty spots have been analyzed on different zircon grains from sample RP-1 and observed data are presented in Table 7.3, whereas the Concordia diagram and weighted average age represented in figure 7.10. The Th/U ratio varies between 0.39–1.44, matching features typical of magmatic origin [393]. On the Concordia diagram (Fig.7.10b), all the age data gathered near the 1600 Ma, with two dates, lie over the Concordia line. However, the weighted average age plot shows 1629±6 Ma (MSWD=1.4) validly constraining the magmatic emplacement event.

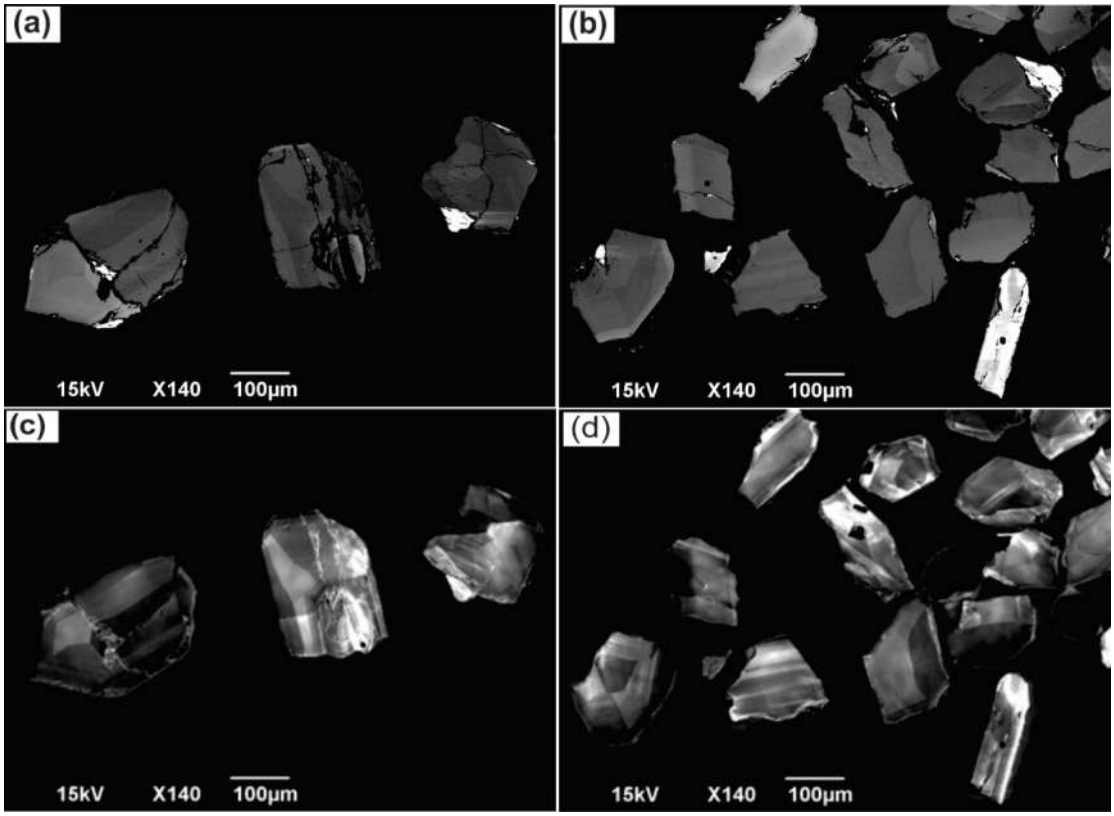

Figure 7.9(a & b) Representative Back-scattered electron (BSE) image; (c & d) Cathodoluminescence (CL) images of zircons with different zoning patterns and metamictised mantle of zircons from mafic granulites from the Daltonganj area.

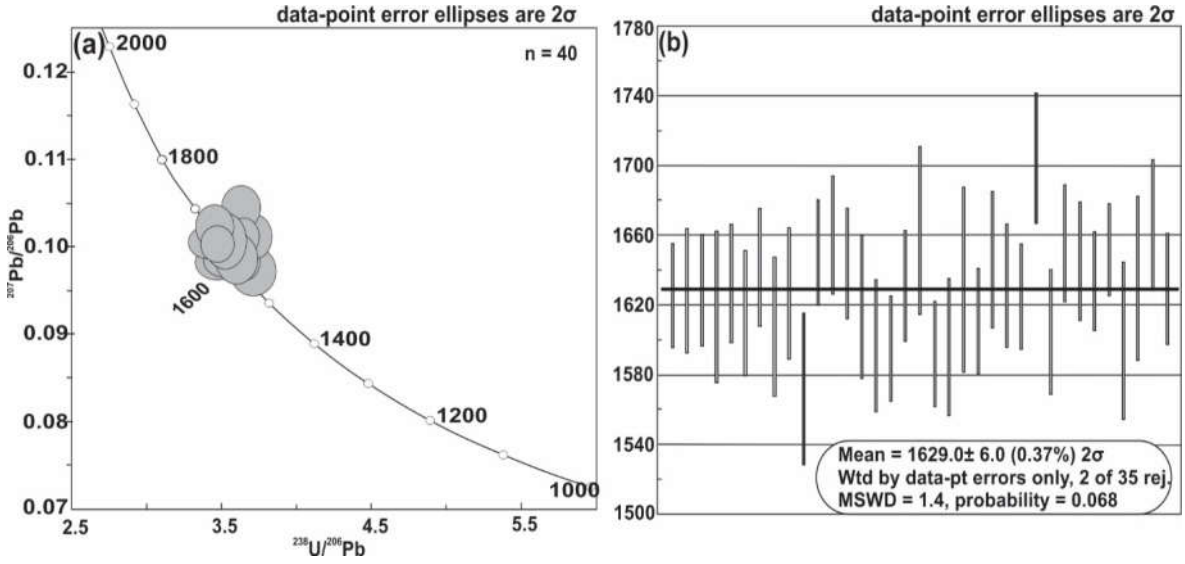

Figure 7.10(a) Analytical data from the pelitic granulite (RP-1) plotted in Tera-Wasserburg Concordia graph. (d) Weighted average age of mean age at 1629.0±60 Ma, with MSWD = 1.4, probability = 0.068.

Table 7.1 Representative electron microprobe analyses and structural formula of monazite (on 4 Oxygen basis).

	R-91-97						R-91-96					
	8/2	10/2	11/2	12/2	13/2	14/2	1/2	2/2	3/2	4/2	5/2	7/2
SiO_2	0.625	1.215	0.486	0.409	0.635	0.434	0.337	0.495	0.266	0.577	0.537	0.266
P_2O_5	30.941	29.738	29.907	30.351	30.365	29.583	30.255	29.495	30.509	29.617	30.210	30.509
CaO	0.840	1.188	0.665	1.108	1.128	1.136	0.916	0.899	0.663	0.840	1.027	0.663
Y_2O_3	1.456	1.408	2.042	1.446	1.406	1.648	0.914	1.068	0.808	1.025	1.162	0.808
La_2O_3	16.125	15.688	15.322	15.446	15.491	15.350	15.692	15.931	16.568	15.430	15.722	16.568
Ce_2O_3	26.629	26.354	26.354	26.265	26.257	26.012	28.866	27.217	28.270	28.564	27.485	28.270
Pr_2O_3	3.135	2.877	3.188	3.117	2.961	3.028	3.311	3.230	3.302	3.088	3.260	3.302
Nd_2O_3	9.910	10.690	10.470	9.830	10.964	11.230	10.466	10.326	10.556	11.023	10.447	10.556
Sm_2O_3	1.850	1.767	1.494	1.670	1.518	1.540	1.808	1.838	1.895	1.836	1.808	1.895
Eu_2O_3	1.320	1.323	1.198	1.441	1.430	1.429	1.466	1.491	1.432	1.393	1.429	1.432
Gd_2O_3	1.262	1.350	1.193	1.265	1.038	1.216	1.181	1.309	1.175	1.272	0.988	1.175
PbO	0.261	0.440	0.423	0.442	0.394	0.419	0.316	0.463	0.361	0.258	0.434	0.361
ThO_2	3.526	4.355	5.690	5.510	4.747	5.054	3.921	4.796	3.707	3.516	4.794	4.569
UO_2	0.280	0.674	0.348	0.376	0.564	0.431	0.258	0.779	0.390	0.279	0.772	0.390
Total	**98.158**	**99.068**	**98.780**	**98.675**	**98.898**	**98.509**	**99.703**	**99.337**	**99.903**	**98.719**	**100.075**	**100.764**
Si	0.026	0.047	0.019	0.016	0.026	0.020	0.014	0.018	0.010	0.024	0.020	0.011
P	1.007	0.990	1.001	1.007	1.007	1.001	1.005	1.001	1.008	0.990	1.005	1.007
Ca	0.036	0.049	0.028	0.042	0.043	0.043	0.038	0.036	0.028	0.036	0.040	0.028
Y	0.030	0.031	0.048	0.030	0.029	0.026	0.019	0.023	0.015	0.024	0.028	0.014
La	0.232	0.226	0.222	0.224	0.226	0.224	0.226	0.228	0.232	0.223	0.227	0.248
Ce	0.396	0.384	0.384	0.381	0.381	0.389	0.400	0.396	0.412	0.403	0.396	0.414
Pr	0.045	0.039	0.045	0.043	0.041	0.039	0.047	0.045	0.047	0.043	0.047	0.047
Nd	0.142	0.148	0.146	0.139	0.155	0.151	0.146	0.144	0.144	0.157	0.144	0.144
Sm	0.024	0.022	0.021	0.022	0.020	0.018	0.023	0.022	0.025	0.024	0.025	0.024
Eu	0.020	0.017	0.017	0.018	0.020	0.021	0.019	0.021	0.018	0.019	0.018	0.020
Gd	0.014	0.016	0.012	0.014	0.012	0.011	0.014	0.019	0.014	0.014	0.012	0.012
Pb	0.002	0.003	0.003	0.003	0.003	0.003	0.002	0.003	0.003	0.002	0.003	0.003
Th	0.031	0.044	0.049	0.047	0.040	0.038	0.040	0.050	0.040	0.031	0.040	0.048
U	0.005	0.007	0.005	0.005	0.005	0.007	0.003	0.008	0.004	0.003	0.009	0.005
Total	2.010	2.023	2.000	1.991	2.008	1.991	1.996	2.014	2.000	1.993	2.014	2.025
Age (Ma)	**1333**	**1492**	**1405**	**1481**	**1348**	**1460**	**1494**	**1409**	**1614**	**1322**	**1331**	**1413**
Age err	**65**	**49**	**48**	**51**	**47**	**51**	**65**	**44**	**63**	**64**	**43**	**50**

Weighted mean age **1424 ± 64 Ma** (n = 6, MSWD = 1.4, probability = 0.21). Age **1390 ± 56 Ma** (n = 6, MSWD = 1.2, probability = 0.30).

Table 7.1 (Cont.) Representative electron microprobe analyses and structural formula of monazite (on 4 Oxygen basis) of sample R-91-97.

	7/1	8/1	10 /1	11/1	15/1	16/1	19 /1	21 /1	22 /1	23 /1	24 /1	26 /1	28 /1	30 /1
SiO_2	bdl	bdl	1.209	0.441	bdl	bdl	bdl	7.453	1.768	0.954	bdl	bdl	bdl	bdl
P_2O_5	26.345	26.542	25.088	26.354	27.155	27.154	26.846	28.317	26.676	29.817	27.345	27.145	27.321	27.548
CaO	1.141	0.998	0.828	1.748	1.125	1.094	1.180	0.863	0.608	1.252	1.202	1.143	1.313	0.826
Y_2O_3	1.849	1.191	0.401	1.729	2.034	1.065	1.741	1.587	0.565	0.993	2.096	2.485	2.088	1.890
La_2O_3	14.710	14.887	15.046	14.477	14.773	14.735	15.009	14.665	16.454	15.780	15.453	15.018	14.735	14.243
Ce_2O_3	25.125	25.846	26.025	25.124	25.632	26.876	26.394	24.856	26.066	26.859	27.366	26.524	26.142	27.512
Pr_2O_3	6.379	6.610	6.274	5.962	6.434	6.426	6.272	4.981	6.039	5.610	6.151	6.223	6.091	6.297
Nd_2O_3	11.324	11.325	10.785	10.583	11.402	11.717	11.460	8.751	11.915	10.138	11.283	11.879	11.252	12.016
Sm_2O_3	2.570	2.668	1.955	2.552	2.554	2.575	1.035	1.920	2.229	2.345	2.542	2.697	2.860	2.849
Eu_2O_3	1.416	1.499	1.432	1.320	1.484	1.530	1.648	0.977	1.323	1.198	1.441	1.430	1.659	1.552
Gd_2O_3	0.988	0.953	1.252	0.989	1.262	0.779	1.202	1.143	1.313	0.826	1.155	0.826	0.828	1.180
PbO	0.346	0.335	0.432	0.442	0.390	0.416	0.422	0.387	0.385	0.387	0.294	0.371	0.444	0.276
ThO_2	6.053	5.391	7.204	6.181	5.591	5.297	5.308	3.136	5.406	3.416	4.834	5.076	5.197	3.372
UO_2	0.939	0.917	1.240	1.215	1.115	1.415	1.380	0.987	0.905	1.184	0.960	1.049	1.518	1.009
Total	**99.186**	**99.161**	**99.170**	**99.117**	**100.949**	**101.078**	**99.897**	**100.023**	**101.651**	**100.759**	**101.609**	**101.864**	**101.447**	**100.570**
Si	bdl	bdl	0.046	0.018	bdl	bdl	bdl	0.252	0.052	0.046	bdl	bdl	bdl	bdl
P	0.947	0.943	0.898	0.930	0.940	0.949	0.910	0.941	0.912	0.944	0.933	0.931	0.933	0.944
Ca	0.049	0.043	0.038	0.075	0.048	0.048	0.049	0.041	0.027	0.051	0.051	0.051	0.053	0.051
Y	0.039	0.025	0.009	0.037	0.043	0.023	0.038	0.034	0.012	0.022	0.043	0.011	0.043	0.022
La	0.220	0.225	0.228	0.211	0.217	0.218	0.228	0.214	0.240	0.234	0.232	0.238	0.228	0.234
Ce	0.374	0.391	0.396	0.363	0.383	0.384	0.396	0.359	0.384	0.392	0.406	0.396	0.381	0.392
Pr	0.092	0.097	0.094	0.087	0.093	0.094	0.094	0.076	0.090	0.082	0.092	0.074	0.086	0.082
Nd	0.161	0.163	0.160	0.150	0.162	0.167	0.167	0.114	0.171	0.159	0.165	0.148	0.165	0.159
Sm	0.035	0.036	0.031	0.035	0.035	0.036	0.015	0.024	0.031	0.034	0.034	0.031	0.038	0.034
Eu	0.019	0.020	0.019	0.020	0.020	0.020	0.020	0.014	0.019	0.017	0.019	0.015	0.021	0.017
Gd	0.059	0.054	0.017	0.061	0.071	0.042	0.017	0.015	0.017	0.012	0.015	0.012	0.012	0.012
Pb	0.004	0.004	0.003	0.005	0.004	0.003	0.003	0.003	0.003	0.003	0.002	0.003	0.003	0.003
Th	0.055	0.049	0.065	0.056	0.051	0.064	0.066	0.034	0.065	0.038	0.046	0.058	0.059	0.041
U	0.008	0.008	0.044	0.011	0.010	0.017	0.040	0.038	0.034	0.041	0.038	0.043	0.052	0.041
Total	2.064	2.058	2.048	2.057	2.079	2.064	2.043	2.159	2.057	2.075	2.076	2.011	2.074	2.032
Age	**912**	**980**	**896**	**965**	**994**	**956**	**917**	**945**	**1050**	**1029**	**1049**	**995**	**994**	**985**
Age err	**51**	**57**	**49**	**55**	**54**	**46**	**43**	**55**	**63**	**61**	**48**	**46**	**53**	**60**

Weighted mean age **972 ± 28 Ma** (n = 14, MSWD = 0.55, probability = 0.47); bdl = Below Detection Limit.

Table 7.1 (Cont.) Representative electron microprobe analyses and structural formula of monazite (on 4 Oxygen basis) of sample R-91-96.

	17/1	32 /1	33/1	34 /1	35/1	37/1	38 /1	40 /1	41 /1	43 /1	51 /1	53/1	54 /1
SiO_2	bdl	0.441	bdl	0.782	bdl	bdl	bdl	bdl	0.275	bdl	0.782	bdl	bdl
P_2O_5	26.956	26.354	27.655	29.249	27.635	27.658	26.426	27.345	26.479	27.154	29.249	26.365	27.635
CaO	1.113	1.748	1.283	0.854	1.010	1.166	1.159	1.195	1.059	1.094	0.854	1.155	1.010
Y_2O_3	2.370	1.729	2.383	0.599	2.124	2.219	2.243	2.021	1.170	1.065	0.599	2.329	2.124
La_2O_3	14.819	14.477	15.229	15.892	14.245	14.124	15.354	15.186	15.373	14.735	15.892	15.264	14.245
Ce_2O_3	24.654	25.124	25.355	26.560	26.635	25.790	26.867	24.963	24.963	26.876	26.560	25.123	26.635
Pr_2O_3	5.623	5.962	5.612	3.162	6.171	6.086	6.187	5.914	6.094	6.426	3.162	6.340	6.171
Nd_2O_3	10.980	10.583	11.016	10.094	11.015	11.175	9.125	11.787	11.245	11.717	10.094	11.460	11.015
Sm_2O_3	2.683	2.552	2.414	1.659	2.389	2.564	2.672	2.631	2.649	2.575	1.659	2.646	2.389
Eu_2O_3	1.429	1.320	1.321	1.416	1.384	1.138	1.491	1.432	1.393	1.530	1.416	1.464	1.384
Gd_2O_3	1.350	0.989	1.193	0.953	0.998	1.748	1.252	1.313	0.826	0.779	0.953	1.125	0.998
PbO	0.413	0.442	0.337	0.459	0.365	0.398	0.387	0.383	0.266	0.416	0.459	0.437	0.365
ThO_2	4.568	6.181	5.658	6.072	5.098	5.500	5.570	5.228	5.802	5.297	6.072	5.577	5.098
UO_2	1.448	1.215	0.971	0.591	1.034	1.121	1.050	1.144	0.883	1.415	0.591	1.144	1.034
Total	**98.404**	**99.117**	**100.426**	**98.340**	**100.103**	**100.687**	**99.782**	**100.543**	**98.475**	**101.078**	**98.340**	**100.427**	**100.103**
Si	bdl	0.018	bdl	0.034	bdl	bdl	bdl	bdl	0.011	bdl	0.034	bdl	bdl
P	0.955	0.930	0.952	0.980	0.970	0.964	0.910	0.933	0.917	0.949	0.980	0.930	0.970
Ca	0.049	0.075	0.053	0.036	0.041	0.048	0.049	0.049	0.045	0.048	0.036	0.047	0.041
Y	0.051	0.037	0.049	0.014	0.043	0.046	0.038	0.041	0.037	0.023	0.014	0.047	0.043
La	0.208	0.211	0.216	0.227	0.223	0.217	0.228	0.231	0.234	0.218	0.227	0.216	0.223
Ce	0.372	0.363	0.360	0.396	0.381	0.375	0.396	0.251	0.251	0.384	0.396	0.370	0.381
Pr	0.083	0.087	0.081	0.047	0.086	0.086	0.094	0.084	0.084	0.094	0.047	0.147	0.086
Nd	0.154	0.150	0.151	0.144	0.150	0.154	0.167	0.167	0.163	0.167	0.144	0.157	0.150
Sm	0.038	0.035	0.032	0.022	0.032	0.034	0.015	0.036	0.036	0.036	0.022	0.035	0.032
Eu	0.021	0.020	0.018	0.018	0.018	0.018	0.020	0.019	0.017	0.020	0.018	0.019	0.018
Gd	0.076	0.061	0.065	0.012	0.061	0.099	0.017	0.019	0.015	0.042	0.012	0.075	0.061
Pb	0.005	0.005	0.004	0.003	0.004	0.004	0.003	0.003	0.002	0.003	0.003	0.005	0.004
Th	0.041	0.056	0.050	0.058	0.044	0.048	0.050	0.046	0.051	0.064	0.058	0.049	0.044
U	0.013	0.011	0.007	0.007	0.009	0.010	0.040	0.044	0.038	0.017	0.007	0.010	0.009
Total	2.064	2.057	2.038	1.998	2.061	2.103	2.027	1.923	1.901	2.064	1.998	2.107	2.061
Age	**964**	**945**	**958**	**1019**	**983**	**926**	**984**	**933**	**975**	**938**	**990**	**965**	**938**
Age err	**50**	**52**	**62**	**59**	**61**	**58**	**64**	**54**	**51**	**52**	**60**	**51**	**58**

Weighted mean age **962 ± 15 Ma** (n = 13, MSWD = 0.88, probability = 0.57); bdl = Below Detection Limit.

Table 7.1 (Cont.) Representative electron microprobe analyses and structural formula of monazite (on 4 Oxygen basis) of both samples.

	1	2	3	4	5	6	7	8	9	10	11	12	13	14
SiO_2	bdl	bdl	bdl	bdl	0.42	bdl	bdl	bdl	0.72	bdl	bdl	1.21	bdl	0.28
P_2O_5	26.81	25.98	27.56	26.32	27.92	27.83	27.31	26.73	26.18	28.54	27.87	25.19	28.51	28.67
CaO	1.19	0.95	1.06	1.30	0.42	1.14	1.09	0.88	0.61	1.28	1.00	0.83	1.20	1.06
Y_2O_3	2.66	1.33	1.66	0.76	0.39	1.85	2.13	1.83	0.41	2.38	1.19	0.40	2.10	1.17
La_2O_3	15.50	15.88	15.23	15.97	16.67	14.99	15.50	16.26	16.57	15.23	15.39	15.05	15.45	15.37
Ce_2O_3	26.30	26.73	25.15	26.53	25.45	25.64	26.43	26.96	26.16	25.57	26.95	26.27	26.15	25.96
Pr_2O_3	5.95	6.58	6.08	6.13	6.61	6.38	6.18	6.33	6.21	5.81	6.69	6.27	6.15	6.09
Nd_2O_3	11.35	11.80	11.67	11.43	12.30	11.32	11.76	12.24	12.00	11.02	11.60	10.78	11.28	11.24
Sm_2O_3	2.42	2.86	2.63	2.71	2.40	2.57	2.64	2.77	2.48	2.41	2.67	1.96	2.54	2.65
Eu_2O_3	1.35	1.61	1.54	1.37	1.38	1.42	1.52	1.63	1.44	1.32	1.50	1.43	1.44	1.39
PbO	0.35	0.32	0.30	0.38	0.36	0.35	0.38	0.25	0.39	0.34	0.33	0.43	0.29	0.27
ThO_2	5.97	4.99	4.53	5.52	5.64	6.05	5.72	4.17	5.51	5.66	5.39	7.20	4.83	5.80
UO_2	0.90	1.10	1.00	1.29	1.22	0.94	1.12	0.87	1.21	0.87	0.92	1.24	0.96	0.88
Total	100.74	100.13	98.41	99.71	101.18	100.48	101.77	100.94	99.89	100.44	101.50	98.27	100.92	100.84
Si	bdl	bdl	bdl	bdl	0.017	bdl	bdl	bdl	0.030	bdl	bdl	0.051	bdl	0.011
P	0.930	0.920	0.959	0.930	0.953	0.953	0.936	0.929	0.920	0.964	0.951	0.902	0.962	0.965
Ca	0.052	0.043	0.047	0.058	0.018	0.049	0.047	0.039	0.027	0.055	0.043	0.037	0.051	0.045
Y	0.058	0.030	0.036	0.017	0.008	0.040	0.046	0.040	0.009	0.051	0.026	0.009	0.044	0.025
La	0.234	0.245	0.231	0.246	0.248	0.224	0.231	0.246	0.254	0.224	0.229	0.235	0.227	0.225
Ce	0.394	0.409	0.378	0.405	0.376	0.380	0.392	0.405	0.398	0.374	0.397	0.407	0.381	0.378
Pr	0.089	0.100	0.091	0.093	0.097	0.094	0.091	0.095	0.094	0.085	0.098	0.097	0.089	0.088
Nd	0.166	0.176	0.171	0.170	0.177	0.164	0.170	0.180	0.178	0.157	0.167	0.163	0.161	0.160
Sm	0.034	0.041	0.037	0.039	0.033	0.036	0.037	0.039	0.035	0.033	0.037	0.028	0.035	0.036
Eu	0.019	0.023	0.022	0.020	0.019	0.020	0.021	0.023	0.020	0.018	0.021	0.021	0.020	0.019
Pb	0.004	0.004	0.003	0.004	0.004	0.004	0.004	0.003	0.004	0.004	0.004	0.005	0.003	0.003
Th	0.056	0.048	0.042	0.052	0.052	0.056	0.053	0.039	0.052	0.051	0.049	0.069	0.044	0.052
U	0.008	0.010	0.009	0.012	0.011	0.008	0.010	0.008	0.011	0.008	0.008	0.012	0.009	0.008
Total	2.044	2.049	2.027	2.046	2.012	2.027	2.039	2.045	2.033	2.023	2.029	2.036	2.026	2.016
Age (Ma)	**886**	**858**	**787**	**868**	**865**	**875**	**906**	**834**	**893**	**902**	**817**	**883**	**848**	**712**
Age err	**61**	**62**	**67**	**56**	**56**	**59**	**58**	**67**	**58**	**63**	**63**	**48**	**66**	**60**

Weighted mean age **855 ± 31 Ma** (n = 14, MSWD = 0.75, probability = 0.71); bdl = Below Detection Limit.

Table 7.2 LA-ICP-MS zircon U-Pb data of pelitic granulite.

	Spot Label	$^{238}U/^{206}Pb^{*}$ ± 2σ		$^{207}Pb^{*}/^{206}Pb^{*}$ ± 2σ		$^{206}Pb^{*}/^{238}U$ age ± 2σ (Ma)		$^{207}Pb^{*}/^{235}U$ age ± 2σ (Ma)		Th/U	Disc.[1] (%)
1	056D2-1c	3.447	0.107	0.104	0.0016	1642.2	45.1	1664.4	28.2	0.39	1.4
2	057D2-1r	3.412	0.116	0.099	0.0012	1656.9	49.9	1637.0	29.7	0.05	-1.2
3	058D2-2c	3.241	0.075	0.105	0.0015	1733.5	35.1	1728.6	22.7	0.71	-0.3
4	059D2-2r	3.619	0.203	0.102	0.0011	1572.6	78.6	1611.8	47.1	0.07	2.5
5	060D2-3	3.262	0.111	0.105	0.0012	1723.7	51.6	1717.9	30.3	0.12	-0.3
6	061D2-4r	3.386	0.132	0.103	0.0014	1668.1	57.6	1671.5	34.2	0.12	0.2
7	062D2-4c	3.136	0.097	0.105	0.0017	1784.4	48.5	1750.4	29.6	0.41	-1.9
8	065D2-5	3.673	0.217	0.101	0.0013	1552.1	81.9	1590.2	49.4	0.01	2.5
9	066D2-6	3.287	0.092	0.105	0.0018	1712.3	42.2	1709.7	27.7	0.43	-0.2
10	067D2-7	3.576	0.193	0.100	0.0013	1589.7	76.5	1607.7	46.2	0.02	1.1
11	068D2-8r	3.378	0.115	0.105	0.0013	1671.8	50.3	1688.5	30.1	0.71	1.0
12	069D2-8c	3.074	0.086	0.105	0.0016	1815.7	44.5	1770.3	27.2	0.26	-2.5
13	070D2-9r	3.207	0.083	0.099	0.0014	1749.8	40.0	1689.0	25.0	0.02	-3.5
14	071D2-9c	3.227	0.100	0.098	0.0015	1739.9	47.4	1671.6	28.3	0.10	-3.9
15	075D2-10	3.290	0.102	0.104	0.0017	1710.7	46.7	1700.4	29.3	0.21	-0.6
16	076D2-11	3.265	0.091	0.106	0.0016	1722.2	42.5	1727.6	26.9	0.51	0.3
17	077D2-12	3.380	0.098	0.101	0.0016	1670.9	42.8	1656.7	27.3	0.02	-0.8
18	078D2-13	3.007	0.096	0.114	0.0018	1850.9	51.7	1860.6	31.2	0.29	0.5
19	079D2-14	3.257	0.088	0.104	0.0015	1726.2	41.0	1710.5	25.1	0.37	-0.9
20	080D2-15	5.055	0.126	0.105	0.0015	1163.6	26.7	1375.3	22.1	0.03	18.2
21	081D2-16	3.696	0.200	0.104	0.0017	1543.7	74.6	1611.4	46.3	1.54	4.4
22	084D2-17	3.375	0.111	0.102	0.0014	1672.9	48.8	1666.3	29.9	0.02	-0.4
23	085D2-18	3.386	0.105	0.101	0.0014	1668.1	45.7	1658.9	28.2	0.02	-0.6
24	086D2-19	3.206	0.096	0.105	0.0015	1750.3	46.1	1737.6	27.8	0.85	-0.7
25	087D2-20	3.328	0.096	0.101	0.0014	1693.9	43.3	1669.8	26.6	0.01	-1.4
26	088D2-21	3.628	0.112	0.098	0.0015	1569.2	43.3	1574.3	27.6	0.01	0.3
27	089D2-22	3.272	0.095	0.105	0.0020	1719.1	43.9	1717.5	29.4	0.39	-0.1
28	090D2-23	3.324	0.123	0.099	0.0016	1695.6	55.4	1652.6	33.2	0.06	-2.5
29	091D2-24	3.393	0.105	0.101	0.0014	1664.9	45.6	1653.9	28.1	0.05	-0.7
30	092D2-25	3.509	0.190	0.101	0.0013	1616.3	77.7	1626.5	46.4	0.03	0.6
31	095D2-27	3.181	0.089	0.103	0.0015	1762.3	43.3	1724.1	26.9	0.19	-2.2
32	096D2-28c	3.217	0.109	0.106	0.0018	1744.8	52.2	1737.0	32.1	0.44	-0.4
33	097D2-28r	3.358	0.138	0.101	0.0016	1680.3	60.9	1659.6	36.6	0.03	-1.2
34	098D2-29r1	4.264	0.350	0.100	0.0017	1358.2	101.	1468.4	67.4	0.13	8.1
35	099D2-29r2	3.549	0.231	0.105	0.0014	1600.2	92.8	1651.4	55.3	0.19	3.2
36	100D2-30c	3.304	0.109	0.100	0.0015	1704.5	49.6	1669.4	29.9	0.07	-2.1
37	101D2-30r	3.719	0.234	0.101	0.0014	1535.1	86.6	1579.2	53.4	0.01	2.9
38	102D2-31r	3.442	0.151	0.099	0.0015	1644.2	64.2	1628.4	38.0	0.01	-1.0
39	103D2-31c	3.161	0.088	0.103	0.0013	1772.1	43.5	1729.0	26.1	0.53	-2.4
40	104D2-32r	3.290	0.112	0.101	0.0017	1711.0	51.3	1684.1	31.7	0.07	-1.6

Table 7.3 LA-ICP-MS zircon U-Pb data of mafic granulite.

	Spot Label	$^{238}U/^{206}Pb^{*} \pm 2\sigma$		$^{207}Pb^{*}/^{206}Pb^{*} \pm 2\sigma$		$^{206}Pb^{*}/^{238}U$ age ± 2σ (Ma)		$^{207}Pb^{*}/^{235}U$ age ± 2σ (Ma)		Th/U	Disc.(1) (%)
1	007B3-1r	3.441	0.100	0.100	0.0016	1644.8	42.2	1636.2	27.2	1.01	-0.5%
2	008B3-1c	3.527	0.095	0.100	0.0019	1609.0	38.6	1617.3	27.1	1.16	0.5%
3	009B3-2	3.448	0.093	0.100	0.0017	1641.5	39.2	1635.5	26.3	1.28	-0.4%
4	010B3-3	3.505	0.105	0.100	0.0023	1618.0	43.1	1618.3	31.2	1.09	0.0%
5	011B3-4	3.613	0.112	0.100	0.0018	1575.1	43.5	1599.6	29.4	1.03	1.6%
6	012B3-5	3.538	0.099	0.100	0.0019	1604.5	39.9	1609.2	27.8	0.78	0.3%
7	013B3-6	3.432	0.096	0.101	0.0018	1648.2	40.9	1645.2	27.2	1.37	-0.2%
8	014B3-7	3.530	0.099	0.099	0.0021	1607.8	40.0	1607.5	28.6	1.21	0.0%
9	018B3-8	3.592	0.090	0.100	0.0020	1583.4	35.2	1601.9	26.1	0.76	1.2%
10	019B3-9	3.713	0.130	0.097	0.0022	1537.5	48.1	1552.1	34.0	0.98	0.9%
11	020B3-10	3.470	0.097	0.101	0.0016	1632.3	40.5	1640.1	26.4	1.41	0.5%
12	021B3-11	3.471	0.104	0.102	0.0018	1631.9	43.4	1644.3	28.9	1.29	0.8%
13	022B3-12	3.525	0.120	0.101	0.0017	1609.9	48.6	1624.6	31.3	1.05	0.9%
14	023B3-13	3.521	0.113	0.100	0.0022	1611.3	45.8	1614.6	32.0	0.95	0.2%
15	024B3-14	3.474	0.115	0.099	0.0020	1631.0	47.7	1616.0	32.0	1.04	-0.9%
16	027B3-15	3.554	0.100	0.098	0.0016	1598.3	39.8	1596.8	26.1	1.00	-0.1%
17	028B3-16	3.500	0.105	0.100	0.0017	1620.1	43.1	1624.8	27.9	1.08	0.3%
18	029B3-17	3.632	0.123	0.102	0.0027	1567.9	47.5	1609.0	35.3	0.99	2.6%
19	030B3-18	3.565	0.103	0.098	0.0017	1593.9	41.1	1592.4	27.7	0.82	-0.1%
20	031B3-19	3.618	0.116	0.099	0.0021	1573.1	44.8	1582.9	30.9	0.39	0.6%
21	032B3-20	3.619	0.134	0.101	0.0028	1572.9	51.8	1599.4	37.7	0.75	1.7%
22	033B3-21	3.623	0.087	0.099	0.0016	1571.4	33.6	1588.3	23.6	1.33	1.1%
23	037B3-22	3.717	0.100	0.101	0.0021	1535.8	37.0	1583.0	27.6	1.03	3.1%
24	038B3-23	3.552	0.099	0.100	0.0019	1599.1	39.8	1613.0	27.9	1.31	0.9%
25	038B3-24	3.579	0.111	0.100	0.0016	1588.5	43.8	1604.4	28.6	1.44	1.0%
26	040B3-25	3.634	0.105	0.104	0.0021	1567.1	40.5	1626.6	28.8	1.21	3.8%
27	041B3-26	3.524	0.116	0.099	0.0019	1610.4	47.2	1607.8	31.1	1.38	-0.2%
28	042B3-27	3.528	0.109	0.102	0.0018	1608.5	44.3	1629.0	29.6	0.92	1.3%
29	043B3-28	3.633	0.102	0.101	0.0018	1567.6	39.1	1601.0	26.9	1.28	2.1%
30	047B3-29	3.400	0.092	0.101	0.0015	1662.3	39.7	1649.9	25.6	0.93	-0.7%
31	048B3-30	3.479	0.090	0.102	0.0014	1628.5	37.5	1638.8	24.7	1.34	0.6%
32	049B3-31	3.608	0.112	0.099	0.0024	1577.2	43.5	1586.7	31.8	1.04	0.6%
33	050B3-32	3.541	0.103	0.101	0.0025	1603.6	41.3	1617.4	31.2	0.90	0.9%
34	051B3-33	3.458	0.104	0.102	0.0020	1637.4	43.5	1650.5	29.8	1.09	0.8%
35	052B3-34	3.480	0.090	0.100	0.0017	1628.3	37.5	1628.8	25.5	1.28	0.0%